Journal of Solid State Chemistry 184 (2011) 982–989

Contents lists available at ScienceDirect

Journal of Solid State Chemistry

journal homepage: www.elsevier.com/locate/jssc

Controllable synthesis of graphene sheets with different numbers of layers and effect of the number of graphene layers on the specific capacity of anode material in lithium-ion batteries

Xin Tong [a], Hui Wang [a,b,*], Gang Wang [a], Lijuan Wan [b], Zhaoyu Ren [b], Jintao Bai [b], Jinbo Bai [c]

[a] Key Laboratory of Synthetic and Natural Functional Molecule Chemistry (Ministry of Education), College of Chemistry and Materials Science, Northwest University, Xi'an 710069, PR China

[b] National Key Laboratory of Photoelectric Technology and Functional Materials (Culture Base), National Photoelectric Technology and Functional Materials and Application International Cooperation Base, Institute of Photonics and Photon-Technology, Northwest University, Xi'an 710069, PR China

[c] Lab. MSS/MAT, CNRS UMR 8579, Ecole Centrale Paris, 92295 Chatenay Malabry, France

ARTICLE INFO

Article history:
Received 8 November 2010
Received in revised form
15 February 2011
Accepted 3 March 2011
Available online 10 March 2011

Keywords:
Graphene sheets
Lithium-ion battery
Number of layers

ABSTRACT

High quality graphene sheets are synthesized through efficient oxidation process followed by rapid thermal expansion and reduction by H_2. The number of graphene layers is controlled by tuning the oxidation degree of GOs. The higher the oxidation degree of GOs is getting, the fewer the numbers of graphene layers can be obtained. The material is characterized by elemental analysis, thermo-gravimetric analysis, scanning electron microscopy, atomic force microscopy, transmission electron microscopy and Fourier transform infrared spectroscopies. The obtained graphene sheets with single, triple and quintuplicate layers as anode materials exhibit a high reversible capacity of 1175, 1007, and 842 mA h g^{-1}, respectively, which show that the graphene sheets with fewer layers have higher reversible capacity.

1. Introduction

As the major anode material of commercial lithium batteries, graphite has excellent electrochemical properties like charge/discharger reversibility, low and flat working potential similar to that of lithium metal [1]. Yet, it has a low theoretical capacity about 372 mA h g^{-1} [2], which terribly affect the performance of lithium batteries. To meet the increasing demand for batteries with higher energy density, various attempts to explore new electrode materials have been investigated [3–6]. Especially, among all the anode materials, carbonaceous nanomaterials are promising candidates to enhance the reversible capacity of batteries, since their layer structure allows insertion/removal of lithium-ions reversibly [7–10].

Graphene sheets are emerging and extraordinary two-dimensional carbon nanomaterials, attracting tremendous attention from both fundamental research and possible applications [11–13]. This unique nanostructure holds great promise for many technological fields [14–16] including transparent conductive films, nanoelectronic devices and composite materials. In the meantime, graphene sheets possess high surface area to volume ratio, superior electronic transport properties and chemical tolerance that make them suitable for reversible lithium storage in lithium-ion batteries. Recently, graphene sheets and graphene-based composites as anode materials were investigated and exhibited large reversible capacity [17–22]. It is worth noting that the variance of specific capacity using the different quality graphene sheets is detected in previous researches. Furthermore, the electronic structure of graphene layers largely depends on its number of layers [23,24]. Therefore, the effects of the number of graphene layers on the specific capacity as anode material in lithium-ion batteries are worth but never researching.

In this investigation, different degrees of oxidized graphite were prepared and high-quality graphene sheets with a selected number of layers was produced by thermal expansion. The dependence of the reversible capacity on the number of layers of the multilayer graphene sheets is also discussed.

2. Experimental section

2.1. Chemical synthesis of graphene sheets

The typical synthesis process is as follows: (i) to produce Graphite Oxide(GO)by a modified Hummers method [25], (ii) to synthesize Expanded Graphite (EG) using a so-called

* Corresponding author at: Key Laboratory of Synthetic and Natural Functional Molecule Chemistry (Ministry of Education), College of Chemistry and Materials Science, Northwest University, Xi'an 710069, PR China. Fax: +86 29 88303798.
E-mail address: huiwang@nwu.edu.cn (H. Wang).

0022-4596/$ - see front matter © 2011 Elsevier Inc. All rights reserved.
doi:10.1016/j.jssc.2011.03.004

explosion–expansion method and (iii) to obtain graphene sheets (GS) through chemical vapor reduction [26].

2.1.1. Oxidation of graphite

The general method is: firstly, 1 g graphite powders (the mean diameter of 18 μm provided by Mei Ge Electrical Carbon Co., Ltd. China) were poured into the mixture of 92 mL concentrated sulfuric acid (95–98%) and 24 mL nitric acid (65%) in a 500 mL flask(under ice bath). After the suspended solution was strongly stirred at 0 °C for 15 min. Then 6 g $KMnO_4$ (AR) was gradually added in the above mixture solution. The suspended solution was stirred continuously for 1 h. We called this process low temperature oxidation. Subsequently, in order to increase the oxidation degree of the graphite, the mixture was heated to 80 °C for 30 min, and then 92 mL of deionized water was slowly added in. The suspension was stirred at 80 °C for 30 min again. After that, 5 mL H_2O_2 (30%) was added into the solution to reduce the residual permanganate. On completion of the reaction, the mixture was washed with 5% solution of HCl and water until sulfate could not be detected with $BaCl_2$. Finally, the GO powders were dried at 80 °C for 24 h. The dosage of oxidizer was controlled to produce oxidized graphite of different degrees.

2.1.2. Expansion of GO

In this step, the obtained GO powders (400 mg) were loaded in a quartz boat. The quartz boat was placed into a 25-mm internal diameter; 1-m long quartz tube. After the sample was flushed with argon for 30 min (the velocity of argon is 100 mL min^{-1}), the quartz tube was heated to 300 °C for 1 h (at heating rates of 15 °C min^{-1}) in tube furnace under argon flow.

2.1.3. Reduction of EG

Graphene sheets obtained from thermal expansion contain residual −H and −OH groups. Therefore, to remove −H and −OH groups, the as-prepared EG were reduced in a tube furnace by H_2 (the gas flow is consisted of H_2 (40 mL min^{-1}) and argon (60 mL min^{-1})) for 2 h at 500 °C. After the GS was dispersed into ethanol, to remove a small amount of precipitate, post-treatment of sonication and centrifugation is used and then the desired graphene sheets are collected for further characterizations.

2.2. Characterization of graphite, GO, EG and GS

The composition, microstructure and morphology of the graphene sheets was analyzed by Scanning electron microscopy (SEM, a Quanta 400 FEG instrument operated at 25 kV, Oxford INCA 350 detector), atomic force microscopy (AFM, Veeco Instruments Inc., USA)and transmission electron microscopy (JEOL 2011 TEM facility). The specific surface areas of the samples were measured with a surface area analyzer (JW-K) by the adsorption of N_2 at liquid N_2 temperature (BET method). Elemental analysis was carried out by a Perkin-Elmer 2400 series I. CHNS/O analyzer. Fourier Transform Infrared spectroscopies (FTIR) were collected by using a Biorad FTS-60A FT-IR device equipped with a diffuse reflectance unit. Thermo-gravimetric analyzer (TGA) was accomplished by means of an SDT Q600 thermobalance (TA Instruments) under Ar gas flow (100 mL min^{-1}) at a heating rate of 10 °C min^{-1}, using Pt crucibles. The *d*-spacing of the samples was monitored by means of X-ray diffraction (XRD; D8 Advance; Cu/*K*α radiation (λ=1.5406 Å), Bruker, Frankfurt, Germany).

2.3. Electrochemical testing of graphene sheets in lithium-ion batteries

The charge and discharge characteristics of graphene sheets were examined in coin-type cells (CR-2430) using metallic lithium as a counter/reference electrode. The working electrodes were prepared by casting slurry containing 80% graphene sheets and 20% poly tetra fluoro ethylene (PTFE) in N-methyl-2-pyrrolidone (NMP) solvent onto a copper mesh. After vacuum drying at

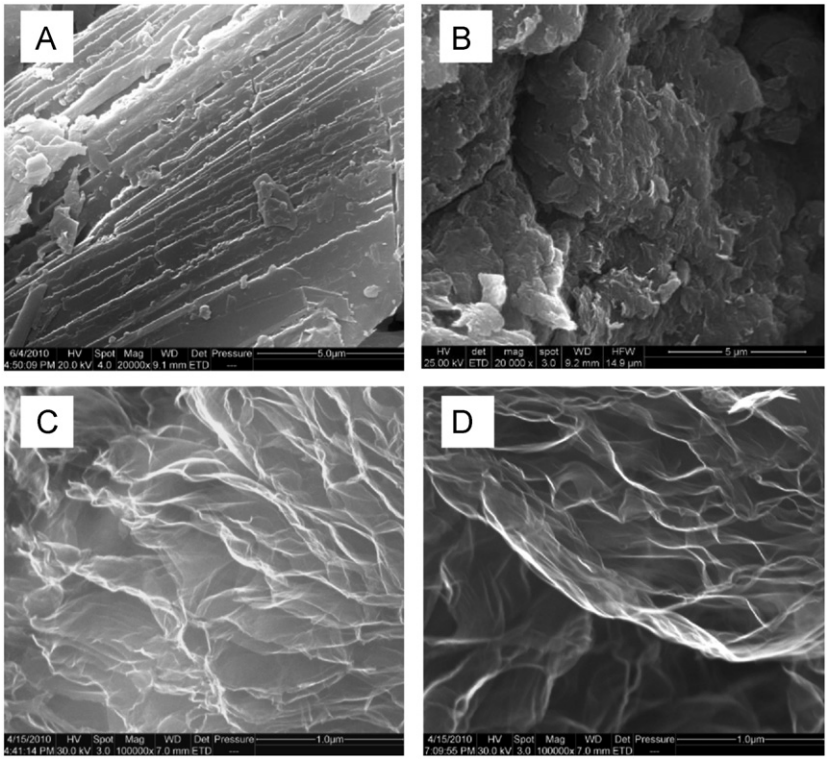

Fig. 1. SEM images of graphite (A), GO (B), EG (C) and graphene sheets (D).

100 °C for about 10 h, the cells were assembled in an argon-filled glove box. The electrolyte was 1 M $LiPF_6$ dissolved in a mixture of diethyl carbonate (DEC), ethylene carbonate (EC) and dimethyl carbonate (DMC) (1:1:1 by volume). The separator was Celgard 2340 microporous polypropylene film. The electrochemical performances were evaluated in a battery test system (LAND CT2001A model, Wuhan Jinnuo Electronics, Ltd.) under a constant current density of 300 mA g^{-1} for a voltage scan from 0.005 to 3.0 V. All tests were performed at room temperature.

3. Result and discussions

3.1. Characterization of GO, EG and GS

Fig. 1 shows the scanning electron microscope (SEM) image of the graphite powders, graphite oxides (GO) expanded graphite (EG) and graphene sheets (GS). The typical laminated structure of graphite can be seen from Fig. 1A. Because of the van der Waals forces holding the layers of graphite together, the layers of graphite were arranged in order. The laminated structure was destroyed and some defects emerged in the graphite layers during the oxidation seen from Fig. 1B. During the oxidation process the extended π-bond conjugated systems of the graphite were broken by the inset of hydroxyl, carbonyl, epoxy, and peroxy groups and results in an increase in the *d*-spacing of GO [27–30]. From Fig. 1C and D, the thin wrinkled accordion or worm-like structure morphology of both EG and graphene sheets can be observed. The particles have a fluffy morphology, consisting of randomly aggregated, thin and wrinkled sheets loosely associated with each other. Most of the graphite oxide has been efficiently exfoliated to separated ultrathin graphene sheets during the above process. And the graphene sheets were agglomerated and overlapped [21,31].

The aforesaid process can be investigated from the FTIR spectra of GO, EG and graphene sheets in Fig. 2. Comparing with the graphite powders (which is infrared-inactive and the detailed data was not shown), the GO exists more absorption peaks. For GO, the broad and intense band at 3422.10 cm^{-1} and the peak at near 1627.69 cm^{-1} in the spectrum of GO are possibly attributed to the stretching vibrations and bending vibrations of OH groups [27], due to the presence of bound water, inhibited water and structural hydroxyl groups. A relatively strong peak at

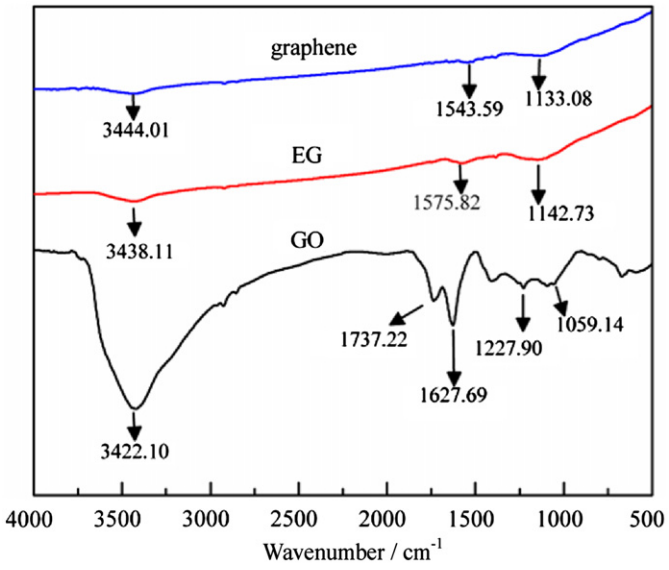

Fig. 2. FTIR spectra of GO, EG and graphene sheets.

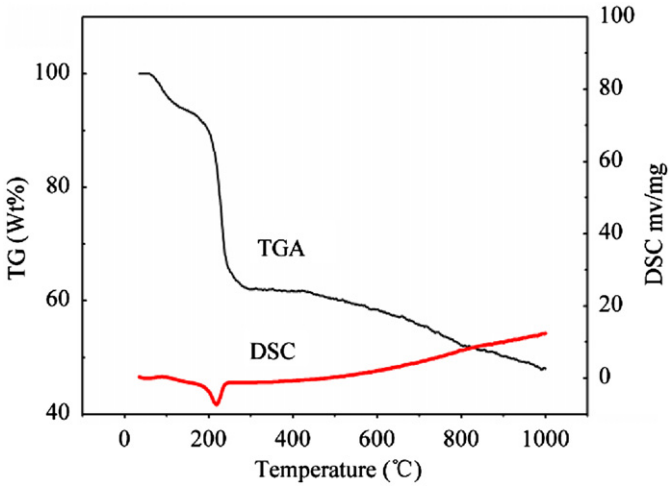

Fig. 3. TG/DSC curves of GO.

1737.22 cm^{-1} may refer to the C=O stretching of COOH groups situated at the edges of the oxidized graphene [28]. The weak peaks located at 1227.90 $cm^{-1}$are most often related to breathing vibrations from epoxy groups. The absorption peak located at 1059.14 cm^{-1} may be assigned to the bending of C–O–C group. This indicates that during oxidation, hydroxyl, carbonyl, epoxy, and peroxy groups were introduced to the edges of basal planes of the graphite structure. After the thermal expansion, the new peaks at 1543.59 cm^{-1} attributed to the skeletal vibration of graphene sheets [18,32] was observed. Here the absorption due to the OH groups was decreased very much in intensity and the peaks at 1735, 1626, 1225 and 1053 cm^{-1} disappeared. Even the oxygen-containing groups at the edges and on the basal planes of graphene sheets owing to the oxidation process can be partly removed during thermal expansion, the H_2 reduction processes which can improve its quality is essential [33]. After the reduction, the intensity of adsorption peaks is getting weaker. This illustrates that the oxygen-containing functional groups derived from the intensive oxidation were eliminated by the thermal expansion and reduction processes.

The course of thermal expansion can also be observed by TGA scans of GO in Fig. 3. The initial weight loss is mainly due to the small amounts of inter-lamellar water evaporation. A sharp mass loss at about 200 °C, accompanying a strongly exothermic DSC peak, is approximately 30% of the initial GO mass. The rapid mass loss is owing to the decomposition of oxygen-containing groups in the GO as CO_2 and H_2O [31,34], along with the expansion–exfoliation process in GO. When the decomposition rate of the epoxy and hydroxyl sites of GO exceeds the diffusion rate of the evolved gases, exfoliation takes place to yield pressures that exceed the van der Waals forces holding the graphene nanosheets together [31]. In our experiment, at approximately 240 °C explosive volume of expansion caused by a vigorous release of gas can be obviously observed in the quartz tube. For this explosive decomposition reaction, exfoliation took place and the graphene sheets can be obtained.

3.2. Synthesis of graphene with different layers

We can control the dosage of oxidizer to produce different degrees of oxidized graphite. The mass ratio of graphite and $KMnO_4$ in GO1, GO2 and GO3 (the oxidation degrees of GO1–GO3 are relatively higher) are 1:3, 1:4, and 1:6, respectively.

The different oxidation degree of GO can be recognized by the color of GO suspension. Seen from the photos of the GOs in Fig. 4a,

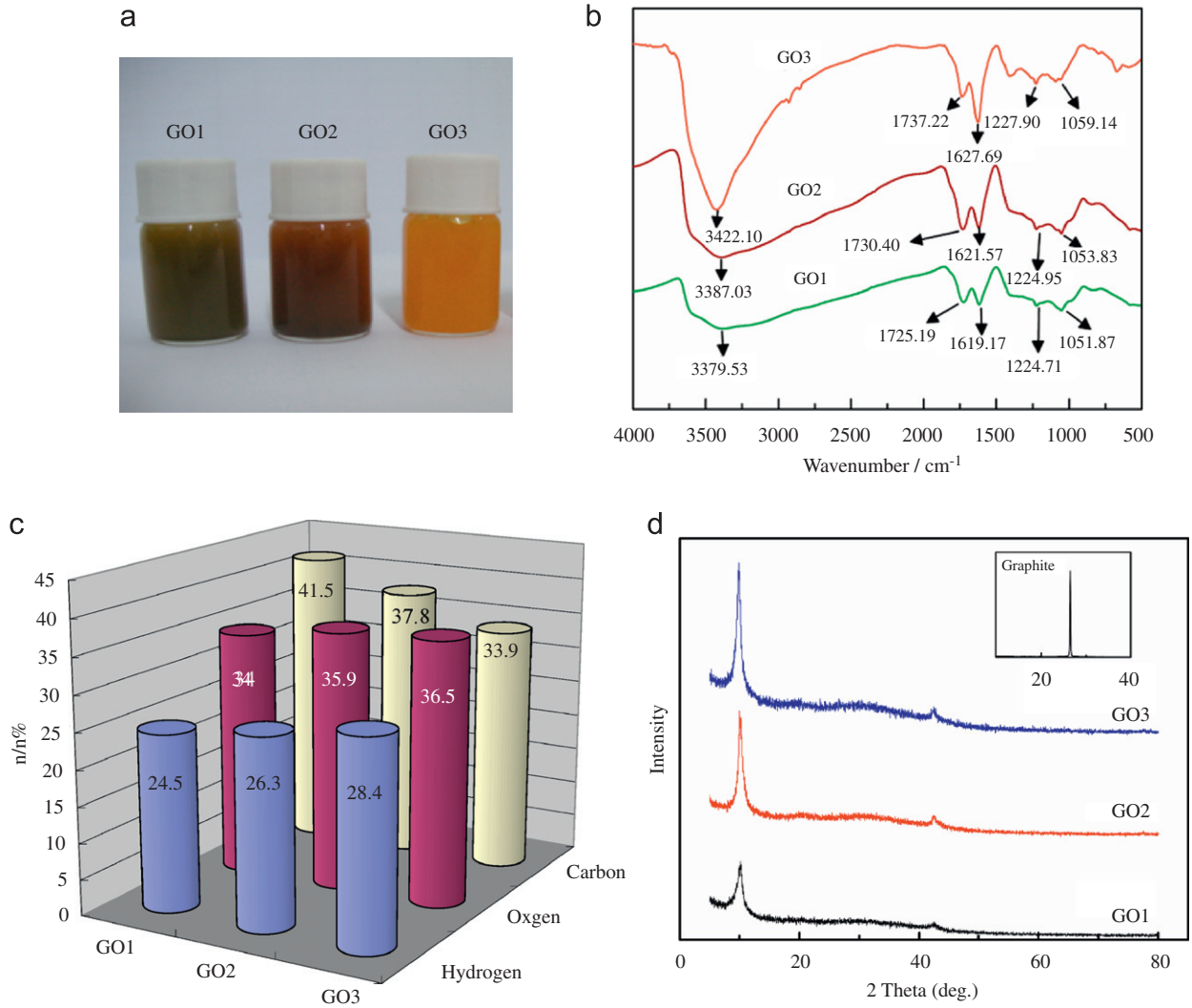

Fig. 4. The photos of different GO suspension: (a) GO1, partial oxidized, GO2, inadequacy oxidized, and GO3, fully oxidized, (b) FTIR spectra of GO1, GO2, and GO3, (c) atomic composition of GOs (from left to right: GO1, GO2 and GO3) and (d) X-ray diffraction patterns of GO1, GO2, and GO3. The inset shows the X-ray diffraction pattern of graphite.

the colors of GO1, GO2 and GO3 are green yellow, brownish red and light yellow/orange, respectively. This is a convenient and effective method for identifying the oxidation degree of GO. We can illustrate the validity of this method by the FTIR spectroscopy and elemental analysis of GOs.

Seen from Fig. 4b, the curves of the samples are similar in shape. However, there are prominent changes in the spectra of the different oxidation degree GOs. The intensity of FTIR adsorption peaks has increased and their peak position shifted to a longer wavelength range with the increase of the oxidizer dosage. Augment of the dosage of oxidizer would be propitious to the formation of hydroxyl, carbonyl and epoxy groups during the oxidation process so as to increases sample's oxidation.

Owing to GOs consist of carbon, oxygen, and hydrogen, the C/O ratio can be seem as a convenient measure of the oxidation degree of GOs [32] (the C/O ratio analyzed by the EA is the atomic ratio of carbon and oxygen). The degree of oxidation increases with the dosage of oxidizer seen from Fig. 4c, a concomitant decrease in the C/O ratio: GO1: 1.222, GO2: 1.052, GO3: 0.962. However, GO is a hygroscopic material and the error that the adsorbed water contributes to higher oxygen content should be considered [32,35]. On the other hand, the producing and handling anhydrous samples is difficult and the change trend of the relative C/O ratio is required. Therefore, we have performed the analysis on air-dry samples equilibrated at the same (50%) relative humidity as applied for measurements, and the relative C/O ratio of different samples with the same inaccuracy is obtained. The results that the oxygen and hydrogen content of GO increases with the degree of oxidation are in accordance with the FTIR. After the course of explosion–expansion and chemical vapor reduction by H_2, the elemental analysis (atomic C/O ratio, 15.5) of the graphene sheets revealed the elimination of most of the oxygen-containing functional groups and residual water. The samples have a lower oxygen content to that of conventional thermally exfoliated GSs (atomic C/O ratio, 10.3) [35]. Theoretical calculations of the reduction of graphene oxide suggest that reduction below 6.25% of the area of the graphene oxide (C/O ratio, 16) may be difficult in terms of removing the remaining hydroxyl groups [36].

X-ray diffraction patterns of the graphite and several graphite oxide samples are recorded in Fig. 4d. Raw graphite sample contained a very sharp and high intensity peak at 26.46° (002) with the layer-to-layer distance (*d*-spacing) of 0.336 nm. After the oxidation treatment, the feature diffraction peak of GO appears at approximately 10° (GO1:10.16°, GO2:10.06° and GO3:9.92°). This fact indicates that the laminar structure with larger *d*-spacing is

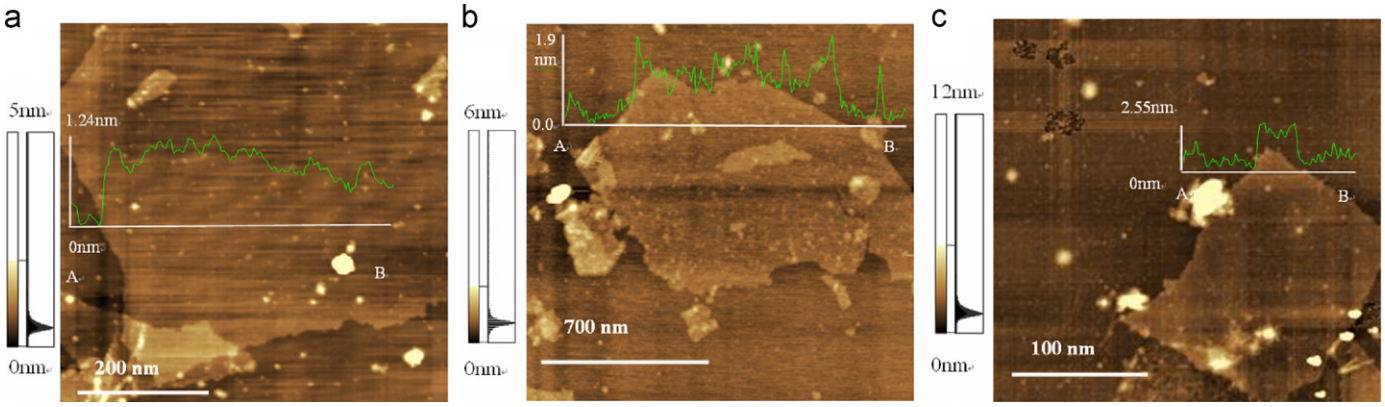

Fig. 5. The AFM images of graphene oxide: (a) GO3, (b) GO2, and (c) GO1.

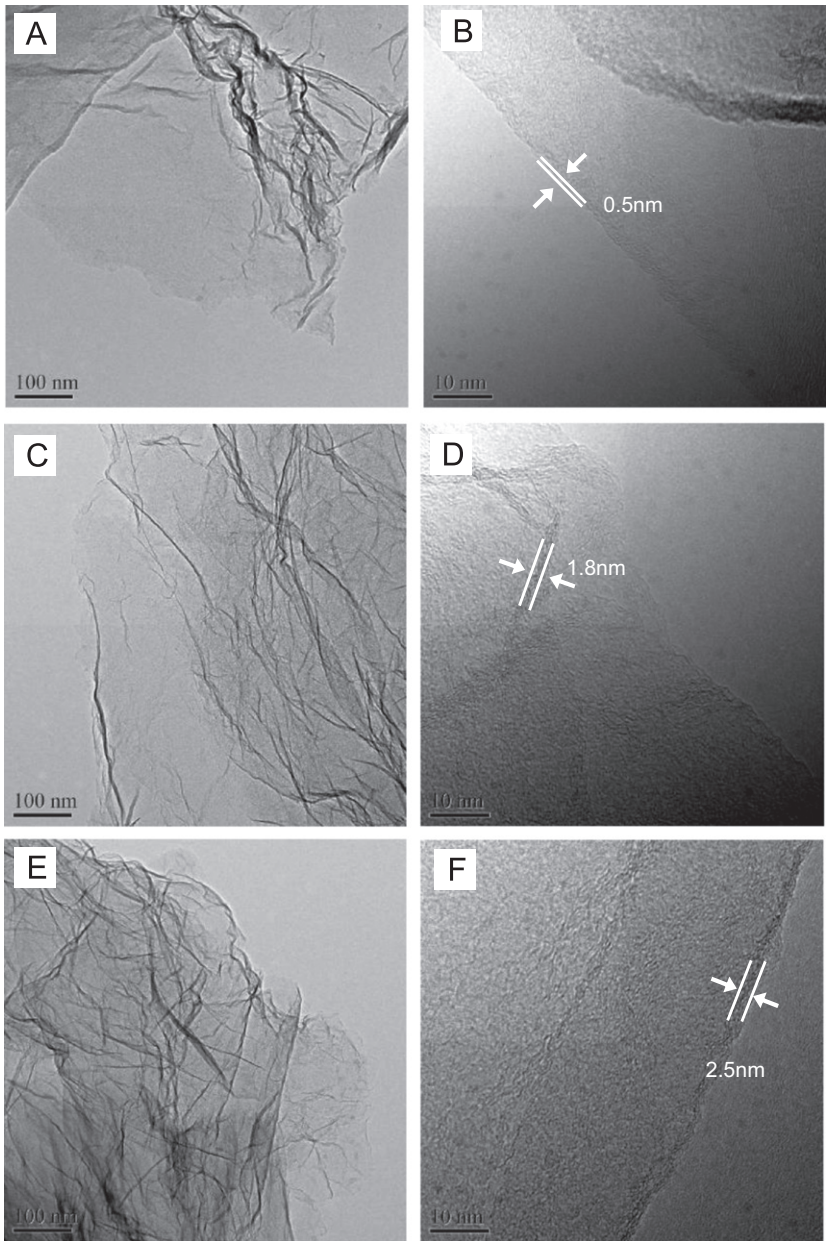

Fig. 6. TEM images of graphene sheets derived from GO3 (A: low magnification and B: high magnification), graphene sheets derived from GO2 (C: low magnification and D: high magnification) and graphene sheets derived from GO1 (E: low magnification and F: high magnification).

observed in graphite oxide. Due to increase in the amount of oxygen-containing functional groups and intercalated water between the layers [27], the intensity and *d*-spacing of the graphite oxide samples (the *d*-spacing: GO1: 0.870 nm, GO2: 0.879 nm and GO3: 0.891 nm) increased with the increase of the oxidizer dosage.

AFM characterization has been the most direct method of quantifying the thickness of samples. In our works, the GO powders are treated with the sonication at concentrations of 1 mg/mL in water and such exfoliation can produce stable dispersions of very thin graphene oxide sheets in water [35,37]. Because of the presence of epoxy and hydroxyl groups on both sides of the surface, the thickness of the graphene oxide sheets is approximately 1.24 nm seen from Fig. 5a and corresponding with the thickness of the single graphene oxide sheets in the early literature [35,38]. With the increases of the degree of oxidation, the thickness of GO2 and GO1 became thickened and the samples of GO1and GO2 consists more sheets than GO3. These results indicate that GOs with fully oxidized are easier to exfoliate and generate single graphene oxide sheets.

In order to obtain the structural information of our graphene sheets, we performed a large number of TEM observations. Fig. 6 shows the typical TEM images of the graphene sheets derived from GO3, GO2 and GO1. The graphene sheets are not perfectly flat but exhibit intrinsic microscopic roughening in low-magnification TEM image in Fig. 6A, C, and E. The graphene sheets look like transparent thin paper structure with some folds. Seen from the low-magnification TEM images, with the increase of the oxidation degree, there are more folds and the thickness of graphene sheets seem to become thickened. In the HRTEM images the thickness and interlayer spacing of graphene can be estimated owing to the folded structure of graphene edges when the layers become almost parallel to the incident electron beam [39]. Seen in Fig. 6, the thickness of the graphene sheets derived from GO3, GO2 and GO1 are approximately 0.5, 1.9 and 2.5 nm, respectively. According to the thicknesses of single-, double-and triple-layer graphene sheets are approximately 0.57, 1.25 and 1.83 nm [21,26], respectively, the as-prepared graphene sheets derived from GO3, GO2 and GO1 are single-layer, triple-layer, and quintuplicate-layer graphene sheets, respectively.

The thicknesses of 100 sheets were measured, and the histogram is shown in Fig. 7. We find that when the oxidation degree of GOs is getting higher, the single and few-layers graphene sheets can be observed more times. Derived from GO3, GO2 and GO1, roughly 80% of the final as-prepared products are single-layer, triple-layer, and quintuplicate-layer graphene, respectively.

The degree of exfoliation of GO is also characterized by the surface areas measured using the BET method by nitrogen gas adsorption [40]. The specific surface area is related to the number of graphene layers [20,21,31]. In Table 1, the specific surface area of graphene sheets derived from GO1, GO2 GO3 is 447.56, 503.24, 594.28 $m^2\,g^{-1}$. Our obtained graphene sheets, which were agglomerated and overlapped, are smaller than the theoretical ones (2620 $m^2\,g^{-1}$). Nevertheless, the theoretical specific surface area of graphene sheets only exists in a hypothetical case where no overlap of sheets occurs and all surfaces are exposed. The results are roughly agreed with the published data (single layer, 600 $m^2\,g^{-1}$ [31] and four layers, 492.5 $m^2\,g^{-1}$ [21]). It is obvious that the graphene sheets obtained derived from GO3 have fewer layers compared with the graphene sheets derived from GO2, GO1.

As can be seen from the above results, during the oxidation of graphite the intensity of oxidation has been enhanced with the increase of the dosage of oxidizer. As shown in Scheme 1, the fully oxidation easily causing configuration changed from a planar sp^2-hybridized to a distorted sp^3-hybrized geometry. More oxygen-containing groups such as epoxy and hydroxyl are introduced on or between the layers. Only when the pressure caused by the decomposition of oxygen-containing groups in the GO counteract the van der Waals binding energy holding the graphene sheets together, can the GO be split into graphene sheets. The intercalating species such as sulfur, nitrogen, and chlorine-containing compounds do not participate in the exfoliation [31].

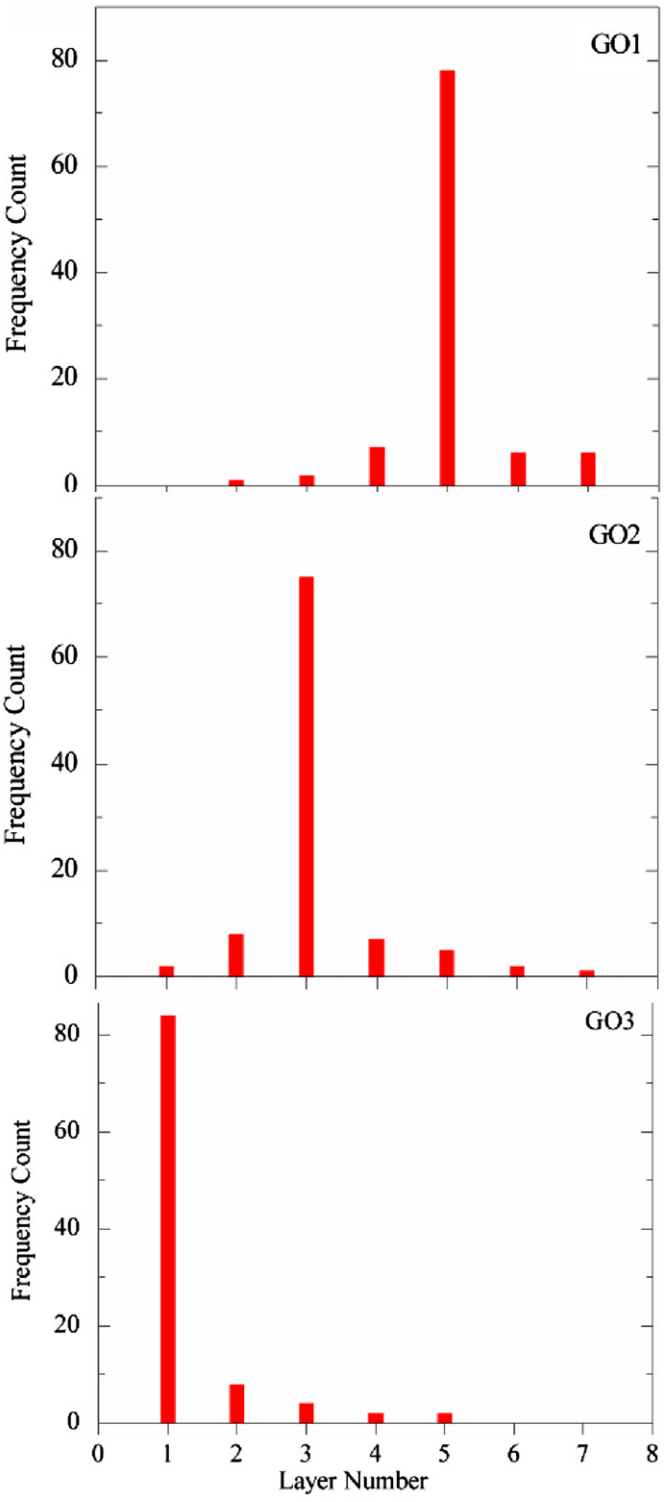

Fig. 7. Statistics of layer numbers of the graphene sheets prepared from GO with different oxidation degree.

Table 1
Specific surface areas of graphite and graphene sheets derived from GO1, GO2 and GO3.

Sample	Graphite	Graphene sheets derived from		
		GO1	GO2	GO3
Specific surface area ($m^2 g^{-1}$)	7.92	447.56	503.24	594.28

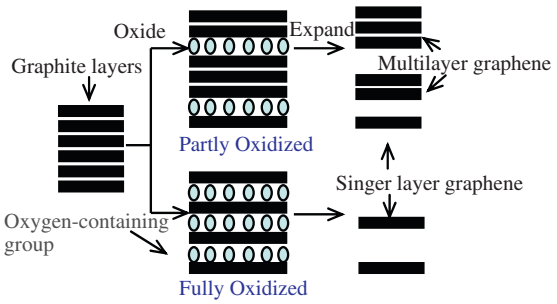

Scheme 1. The schematic sketch of formation process of graphene sheets with different numbers of layers.

The exfoliation degree of graphene sheets is mainly due to the different oxidation degree of the GO [26]. Obviously, the expanding of graphene sheets derived from GOs with fully oxidized is more tempestuous than that derived from GO with partial oxidized. Due to the number of layers in graphene sheets is mainly determined by the exfoliation process, the single and few-layers can be obtained more easily in the samples derived from GOs with fully oxidized.

3.3. *Effect of graphene layers on the storage capacity as anode material in lithium-ion batteries*

The electrochemical data of the graphene sheets anode material are shown in Fig. 8. Fig. 8A–C present the first, second and the 20th discharge/charge profiles of the prepared graphene sheets at the current density of 300 mA g^{-1}. The graphene sheets shown in Fig. 8A–C are obtained from GO3, GO2, GO1 (the graphene sheets with single, triple and quintuplicate layers). The shape of the charge (lithium intercalation)–discharge (deintercalation) curves of the graphene sheets is similar to the previous articles [17–21] such as large charge/discharge voltage hysteresis, high irreversible capacity and without distinguishable plateaus. Typically, in the charge process (lithium intercalation), the slope of the curve starts approximately 2.5 V, and has large specific capacities (> 70%) below 0.5 V. The capacity lower than 0.5 V should be ascribed to the lithium intercalation into the graphene layers. The lithium-ions can be adsorbed on both sides of the graphene sheets. However, the capacity above 0.5 V could be as the result of the Faradic capacitance both on the surface and the edge sites of graphene sheets [17].

It can be seen that the voltage curve of the first charge process is obviously different from the second one. The first-cycle charge capacities of the obtained graphene sheets with single, triple and quintuplicate layers are 2334, 2035, 1676 mA h g^{-1}, respectively. The previous reports [41,42] ascribed the irreversible capacity to the electrolyte decomposition and formation of SEI layer, both of which take place simultaneously at graphene surfaces. It is understandable that the irreversible capacity changes over the specific surface area. Single-layer graphene sheets with the highest specific surface have the maximum specific charge capacity.

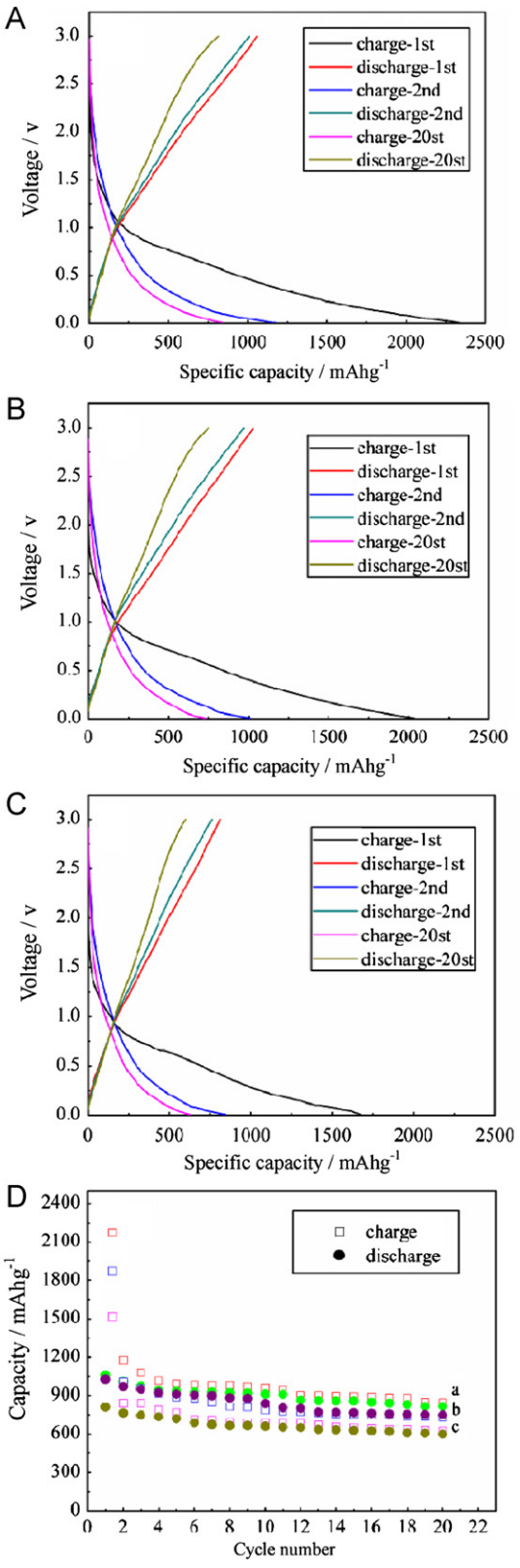

Fig. 8. Discharge/charge profiles of: (A) graphene sheets derived from GO3, (B) graphene sheets derived from GO2, (C) graphene sheets derived from GO1 at the current density of 300 mA g^{-1} and (D) capacity with cycle numbers at a the current density of 300 mA g^{-1} (A) graphene sheets derived from GO3, (B) graphene sheets derived from GO2 and (C) graphene sheets derived from GO1.

During the second cycle, the reversible capacity at a current density of 300 mA g^{-1} is 1175, 1007, and 842 mA h g^{-1} for graphene sheets with single, triple and quintuplicate layers.

The reversible capacity of graphene sheets with different layers varies regularly with the change of layers numbers. It matches well enough with the results on the publicized literature that the more lithium insertion active sites can be supplied by the graphene sheets with fewer layers [20,21,43]. Obviously, the specific surface area is getting larger as the numbers of graphene layers decreased. Larger capacity may be related to the larger specific surface area. On the other hand, nano-cavities between graphene sheets due to scrolling and crumpling can also contribute to reversible capacity to the graphene sheets. The graphene sheets with fewer layers can provide more lithium insertion active sites, such as edge-typesites, to store lithium-ion. Hence the reversible capacity of graphene sheets with different layers mainly depends on the number of layers. The graphene sheets with fewer layers can have an energy storing capability higher than that with numerous layers.

The cyclability of graphene sheets electrode was examined shown in Fig. 8D. After 20cycles, the graphene anode still maintained a specific capacity of 846, 730, 628 mA h g^{-1} for graphene sheets with single, triple and quintuplicate layers, that is, about 70% retention of the reversible capacity. It demonstrates that chemically prepared graphene sheets exhibit excellent electrochemical properties compared to graphite anodes.

In the case of graphene sheets with different layers, their preparation is simple and the reversible capacity is high, but their high irreversible capacity, without distinguishable plateaus and voltage hysteresis needs to be improved.

4. Conclusions

We have developed an efficient method of oxidation of graphite. Unlike the traditional method, the oxidization time of the process is only approximately 3 h. Moreover, the oxidation degree of GOs can also be controlled. On the basis of controlled process of oxidation of graphite, the high quality graphene sheets with different numbers of layers can be obtained. Due to the pressure caused by the gaseous products which are derived from the exothermic decomposition of hydroxyl and epoxide groups of the GO, the number of layers of graphene sheets mainly depends on the oxidation degree of GOs. The higher the oxidation degree of GOs is getting, the fewer the numbers of graphene layers can be obtained. Furthermore, the dependence of the specific capacity on number of layers of multilayer graphene sheets is also discussed. The graphene sheets with fewer layers have higher reversible capacity. It would be reasonable to expect that our findings can be the basis of the further investigation of graphene with different numbers of layers such as the applications in rechargeable lithium-ion battery, opening up enormous opportunities for many new and potentially technological applications.

Acknowledgment

The project was supported by the financial supports of the National Basic Research Program of China (973 Program) (no. 2009CB626611), the International cooperation research program of National Natural Science Foundation of China (no. 21061130551), the Ph.D. Programs Foundation of Ministry of Education of China (no. 20096101110002), the National Natural Science Foundation of China (nos. 20873099 and 10974152), NWU Doctorate Dissertation of Excellence Funds (09YYB04), and NWU Graduate Cross-discipline Funds (07YJC03 and 09YJC28). The authors are also grateful to the State Key Laboratory of Continental Dynamics for the SEM measurements.

References

[1] H. Shi, J. Power Sources 75 (1998) 64–72.
[2] J.M. Tarascon, M. Armand, Nature 414 (2001) 359–367.
[3] O. Crosnier, T. Brousse, X. Devaux, P. Fragnaud, D.M. Schleich, J. Power Sources 94 (2001) 169–174.
[4] H. Jung, M. Park, Y.-G. Yoon, G.-B. Kim, S.-K. Joo, J. Power Sources 115 (2003) 346–351.
[5] N. Dimov, S. Kugino, M. Yoshio, J. Power Sources 136 (2004) 108–114.
[6] L. Yuan, Z.P. Guo, K. Konstantinov, H.K. Liu, S.X. Dou, J. Power Sources 159 (2006) 345–348.
[7] J.-X. Li, Y. Zhao, L.-H. Guan, Electrochem. Commun. 12 (2010) 592–595.
[8] J.-H. Lee, G.-S. Kim, Y.-M. Choi, W.I. Park, J.A. Rogers, U. Paik, J. Power Sources 184 (2008) 308–311.
[9] H. Habazaki, M. Kiriu, H. Konno, Electrochem. Commun. 8 (2006) 1275–1279.
[10] Y.-S. Yang, C.-Y. Wang, M.-M. Chen, Z.-Q. Shi, J.-M. Zheng, J. Solid State Chem. 183 (2010) 2116–2120.
[11] K.S. Novoselov, A.K. Geim, S.V. Morozov, D. Jiang, M.I. Katsnelson, I.V. Grigorieva, S.V. Dubonos, A.A. Firsov, Nature 438 (2005) 197–200.
[12] Y. Zhang, Y.-W. Tan, H.L. Stormer, P. Kim, Nature 438 (2005) 201–204.
[13] A.K. Geim, Science 324 (2009) 1530–1534.
[14] S. Stankovich, D.A. Dikin, G.H.B. Dommett, K.M. Kohlhaas, E.J. Zimney, E.A. Stach, R.D. Piner, S.T. Nguyen, R.S. Ruoff, Nature 442 (2006) 282–286.
[15] S. Watcharotone, D.A. Dikin, S. Stankovich, R. Piner, I. Jung, G.H.B. Dommett, G. Evmenenko, S.-E. Wu, S.-F. Chen, C.-P. Liu, S.T. Nguyen, R.S. Ruoff, Nano Lett. 7 (2007) 1888–1892.
[16] G. Eda, G. Fanchini, M. Chhowalla, Nat. Nano 3 (2008) 270–274.
[17] E. Yoo, J. Kim, E. Hosono, H.-s. Zhou, T. Kudo, I. Honma, Nano Lett. 8 (2008) 2277–2282.
[18] P. Guo, H. Song, X. Chen, Electrochem. Commun. 11 (2009) 1320–1324.
[19] D. Pan, S. Wang, B. Zhao, M. Wu, H. Zhang, Y. Wang, Z. Jiao, Chem. Mater. 21 (2009) 3136–3142.
[20] G. Wang, X. Shen, J. Yao, J. Park, Carbon 47 (2009) 2049–2053.
[21] P. Lian, X. Zhu, S. Liang, Z. Li, W. Yang, H. Wang, Electrochim. Acta 55 (2010) 3909–3914.
[22] C. Xu, X. Wang, L. Yang, Y. Wu, J. Solid State Chem. 182 (2009) 2486–2490.
[23] D.-W. Wang, F. Li, Z.-S. Wu, W. Ren, H.-M. Cheng, Electrochem. Commun. 11 (2009) 1729–1732.
[24] T. Ohta, A. Bostwick, J.L. McChesney, T. Seyller, K. Horn, E. Rotenberg, Phys. Rev. Lett. 98 (2007) 206802.
[25] W.S. Hummers Jr., R.E. Offeman, J. Am. Chem. Soc. 80 (1958) 1339.
[26] Z.-S. Wu, W. Ren, L. Gao, B. Liu, C. Jiang, H.-M. Cheng, Carbon 47 (2009) 493–499.
[27] C. Hontoria-Lucas, A.J. López-Peinado, J.d.D. López-González, M.L. Rojas-Cervantes, R.M. Martín-Aranda, Carbon 33 (1995) 1585–1592.
[28] T. Szabó, O. Berkesi, I. Dékány, Carbon 43 (2005) 3186–3189.
[29] A.B. Bourlinos, D. Gournis, D. Petridis, T. Szabó, A. Szeri, I. Dékány, Langmuir 19 (2003) 6050–6055.
[30] T. Szabó, A. Szeri, I. Dékány, Carbon 43 (2005) 87–94.
[31] M.J. McAllister, J.-L. Li, D.H. Adamson, H.C. Schniepp, A.A. Abdala, J. Liu, M. Herrera-Alonso, D.L. Milius, R. Car, R.K. Prud'homme, I.A. Aksay, Chem. Mater. 19 (2007) 4396–4404.
[32] T. Szabó, O. Berkesi, P. Forgó, K. Josepovits, Y. Sanakis, D. Petridis, I. Dékány, Chem. Mater. 18 (2006) 2740–2749.
[33] Z.-S. Wu, W. Ren, L. Gao, J. Zhao, Z. Chen, B. Liu, D. Tang, B. Yu, C. Jiang, H.-M. Cheng, ACS Nano 3 (2009) 411–417.
[34] H.C. Schniepp, J.-L. Li, M.J. McAllister, H. Sai, M. Herrera-Alonso, D.H. Adamson, R.K. Prud'homme, R. Car, D.A. Saville, I.A. Aksay, J. Phys. Chem. B 110 (2006) 8535–8539.
[35] S. Stankovich, D.A. Dikin, R.D. Piner, K.A. Kohlhaas, A. Kleinhammes, Y. Jia, Y. Wu, S.T. Nguyen, R.S. Ruoff, Carbon 45 (2007) 1558–1565.
[36] D.W. Boukhvalov, M.I. Katsnelson, J. Am. Chem. Soc. 130 (2008) 10697–10701.
[37] S. Stankovich, R.D. Piner, S.T. Nguyen, R.S. Ruoff, Carbon 44 (2006) 3342–3347.
[38] Y. Si, E.T. Samulski, Nano Lett. 8 (2008) 1679–1682.
[39] J.C. Meyer, A.K. Geim, M.I. Katsnelson, K.S. Novoselov, T.J. Booth, S. Roth, Nature 446 (2007) 60–63.
[40] I. Dékány, R. Krüger-Grasser, A. Weiss, Colloid Polym. Sci. 276 (1998) 570–576.
[41] D. Aurbach, J. Power Sources 89 (2000) 206–218.
[42] J. Hu, H. Li, X. Huang, Solid State Ionics 178 (2007) 265–271.
[43] T. Takamura, K. Endo, L. Fu, Y. Wu, K.J. Lee, T. Matsumoto, Electrochim. Acta 53 (2007) 1055–1061.